Title

Second harmonic generation detection of Ras conformational changes and discovery of a small molecule binder

Journal

Proceedings of the National Academy of Sciences of the United States of America, 116(35)

ISSN

0027-8424

Authors

Donohue, Elizabeth
Khorsand, Sina
Mercado, Gabriel
et al.

Publication Date

2019-08-27

DOI

10.1073/pnas.1905516116

Peer reviewed

Second harmonic generation detection of Ras conformational changes and discovery of a small molecule binder

Elizabeth Donohue[a,b], Sina Khorsand[a,b], Gabriel Mercado[b], Kristen M. Varney[c,d,e], Paul T. Wilder[c,d,e], Wenbo Yu[c,d,f], Alexander D. MacKerell Jr[c,d,e,f], Patrick Alexander[g], Que N. Van[g], Ben Moree[b], Andrew G. Stephen[g], David J. Weber[c,d,e], Joshua Salafsky[h,1], and Frank McCormick[a,g,1]

[a]Helen Diller Family Comprehensive Cancer Center, University of California, San Francisco, CA 94158; [b]Biodesy, Inc., South San Francisco, CA 94080; [c]Center for Biomolecular Therapeutics, School of Medicine, University of Maryland, Baltimore, MD 21201; [d]Department of Biochemistry and Molecular Biology, School of Medicine, University of Maryland, Baltimore, MD 21201; [e]Marlene and Stewart Greenebaum Comprehensive Cancer Center, University of Maryland, Baltimore, MD 21201; [f]Department of Pharmaceutical Sciences, School of Pharmacy, University of Maryland, Baltimore, MD 21201; [g]National Cancer Institute RAS Initiative, Cancer Research Technology Program, Frederick National Laboratory for Cancer Research, Leidos Biomedical Research, Inc., Frederick, MD 21702; and [h]Department of Pharmaceutical Chemistry, University of California, San Francisco, CA 94158

Contributed by Frank McCormick, June 28, 2019 (sent for review April 4, 2019; reviewed by Gideon Bollag and Jeff Settleman)

Second harmonic generation (SHG) is an emergent biophysical method that sensitively measures real-time conformational change of biomolecules in the presence of biological ligands and small molecules. This study describes the successful implementation of SHG as a primary screening platform to identify fragment ligands to oncogenic Kirsten rat sarcoma (KRas). KRas is the most frequently mutated driver of pancreatic, colon, and lung cancers; however, there are few well-characterized small molecule ligands due to a lack of deep binding pockets. Using SHG, we identified a fragment binder to $KRas^{G12D}$ and used ^{1}H ^{15}N transverse relaxation optimized spectroscopy (TROSY) heteronuclear single-quantum coherence (HSQC) NMR to characterize its binding site as a pocket adjacent to the switch 2 region. The unique sensitivity of SHG furthered our study by revealing distinct conformations induced by our hit fragment compared with 4,6-dichloro-2-methyl-3-aminoethyl-indole (DCAI), a Ras ligand previously described to bind the same pocket. This study highlights SHG as a high-throughput screening platform that reveals structural insights in addition to ligand binding.

second harmonic generation | KRAS | small G protein | cancer | small molecule inhibitors

The Ras protein family comprises small GTPases that are critical signaling transducers regulating cell proliferation and survival. Ras proteins cycle between an inactive GDP-bound state and an active GTP-bound state in a process regulated by guanine nucleotide exchange factors, which catalyze nucleotide exchange, and GTPase activating proteins (GAPs), which accelerate GTP hydrolysis. In its active state, residues in the switch 1 (amino acids 30 to 38) and switch 2 (amino acids 60 to 76) regions of Ras interact with the γ-phosphate of GTP to adopt a rigid conformation that enables effector binding to proteins, including RAF1 and PI3K. On GTP hydrolysis, switch 1 and 2 regions relax into the inactive conformation, thus losing the binding interface (1, 2). Oncogenic mutations in one of the Ras isoforms (K, H, N) impair GAP-facilitated GTP hydrolysis, thus deregulating Ras signaling and driving tumorigenesis (3, 4).

Ras mutations occur in one-third of human cancers, making it the most commonly mutated oncogenic driver of tumorigenesis. Among the Ras subtypes, Kirsten rat sarcoma (KRas)-driven cancers are particularly aggressive and resistant to traditional therapies, highlighting a great unmet clinical need. Conventional efforts to inhibit oncogenic Ras with small molecules have been largely unsuccessful, leading to its characterization as an "undruggable" protein. Challenges to effectively drugging Ras include its picomolar affinity for GTP/GDP and the lack of obvious additional pockets for ligand binding. Despite these obstacles, technological advances and innovative targeted approaches have contributed to promising developments in Ras drug discovery (1, 4–6). Fragment-based lead discovery has been applied to Ras in several NMR-based screens that identified low-affinity ligands (7–9). Additionally, covalent tethering strategies identified a flexible switch 2 binding pocket that enables irreversible targeting to G12C oncogenic KRas, and extensive efforts are underway to evaluate the therapeutic efficacy of these covalent inhibitors (6, 10–12). However, despite the relevance of oncogenic KRas for human cancer and the significant efforts to date, few well-characterized small molecule noncovalent ligands exist for this protein.

Significance

KRas is the most frequently mutated oncogene in human cancer, and its critical role in tumorigenesis is well established. Historical challenges in targeting KRas have led to its characterization as an "undruggable" target, but recent advances in drug discovery approaches have revealed promising avenues toward the development of small molecule Ras inhibitors. This study describes the successful implementation of second harmonic generation (SHG) as a screening platform to identify a conformational modulator of KRas that binds to a single distinct pocket. This work demonstrates how SHG screening can be applied to both the discovery and characterization of ligands for a high-value oncogenic target.

Author contributions: E.D., G.M., K.M.V., P.T.W., B.M., A.G.S., J. Salafsky, and F.M. designed research; E.D., S.K., G.M., K.M.V., P.T.W., W.Y., P.A., and Q.N.V. performed research; E.D., S.K., G.M., K.M.V., P.T.W., W.Y., A.D.M., P.A., Q.N.V., B.M., A.G.S., D.J.W., J. Salafsky, and F.M. analyzed data; J. Salafsky and F.M. provided scientific guidance; F.M. funded the study; and E.D., A.D.M., A.G.S., J. Salafsky, and F.M. wrote the paper.

Reviewers: G.B., Plexxikon; and J. Settleman, Calico Life Sciences.

Conflict of interest statement: E.D. and G.M. were previously employed at Biodesy, Inc. S.K. is an employee of Biodesy, Inc. A.D.M. is cofounder and Chief Scientific Officer of SilcsBio LLC. B.M. is an employee of Biodesy, Inc. and has equity grants in the company. J. Salafsky is the founder of Biodesy, Inc., where the research was performed. F.M. is a consultant for the following companies: Aduro Biotech; Amgen; Daiichi Ltd; Ideaya Biosciences; Kura Oncology; Leidos Biomedical Research, Inc.; PellePharm; Pfizer Inc.; PMV Pharma; Portola Pharmaceuticals; and Quanta Therapeutics. F.M. has received research grants from Daiichi Ltd and is a recipient of funded research from Gilead Sciences. F.M. is a consultant and cofounder for the following companies (with ownership interest, including stock options): BridgeBio; DNAtrix Inc.; Olema Pharmaceuticals, Inc.; and Quartz. F.M. is Scientific Director of the National Cancer Institute Ras Initiative at Frederick National Laboratory for Cancer Research/Leidos Biomedical Research, Inc.

[1]To whom correspondence may be addressed. Email: frank.mccormick@ucsf.edu or joshua.salafsky@ucsf.edu.

This article contains supporting information online at www.pnas.org/lookup/suppl/doi:10.1073/pnas.1905516116/-/DCSupplemental.

Published online August 9, 2019.

Second harmonic generation (SHG) is a sensitive biophysical technique that detects real-time changes in protein conformation under dynamic conditions (13, 14). In SHG, 2 photons of equal energy are combined by a nonlinear material to emit a single photon with twice the energy. Although most biological molecules are not intrinsically second harmonic (SH) active, they can be rendered so through the chemical incorporation of SHG dye probes (15–17). When SH-active molecules are tethered to a surface and illuminated with high-intensity pulsed 800-nm laser light, the molecules emit an SH signal at 400 nm, and the intensity of this resultant signal is highly dependent on the net average angular orientation of the SHG dye(s) relative to the surface normal (Fig. 1*A*). Since SHG signal changes are proportional to the net SHG dye movement upon ligand binding, this technique sensitively detects relative orientational shifts indicative of protein conformational change(s). Although SHG requires target immobilization, assays are carried out in solution with a monolayer of protein molecules tethered to a glass-supported lipid bilayer, enabling the capture of dynamic changes in real time (17–19). Recent studies have demonstrated that SHG can detect and characterize conformational changes in a variety of biological targets (17–21). In general, when the SH-active biomolecule undergoes a conformational change, the SHG intensity increases as the net orientation of the dye moves toward the surface normal and, conversely, decreases as the dye moves away from this plane (Fig. 1*B*). Ligands that bind or stabilize different conformational states of the protein produce different SHG signal changes relative to the baseline (preligand) signal. As KRas activity is directly governed by its conformational state and recent findings support the presence of dynamic binding pockets (7, 9, 22), we were motivated to implement SHG to screen for conformational modulators that could serve as starting points for drug discovery.

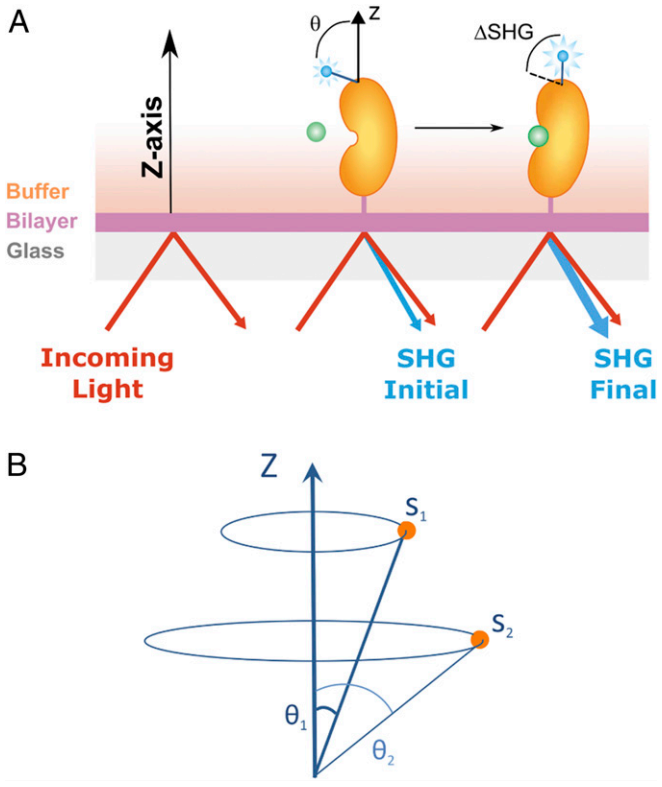

Fig. 1. SHG schematic. (*A*) When a labeled protein tethered to a membrane-coated surface is pulsed with an infrared laser, the SHG probe converts a portion of the incident light into blue light, the SHG signal. The intensity of the SH signal is highly dependent on the orientation of the dye probe relative to the surface normal (*z* axis) and is sensitive to relative changes in the time- and space-averaged orientation of the dye probe that reports on conformational changes. (*B*) A conformational change that alters the orientation of the label in relation to the *z* axis increases or decreases the signal intensity. In general, when the SHG dye shifts away from the *z* axis ($s_1 \rightarrow s_2$), the signal decreases, and when it shifts toward the *z* axis, it increases ($s_2 \rightarrow s_1$).

Results

KRas SHG Assay Development. To identify KRas ligands using SHG, we targeted recombinant His-tagged KRas4b (1-166) carrying the G12D mutation (hereafter referred to as $KRas^{G12D}$). G12D is among the most common activating KRas point mutations, particularly in pancreatic and colon malignancies. Using this construct, we built SHG assays against both the inactive GDP-bound conformation and the active 'GTP'-bound conformation using the nonhydrolyzable analog, GMP-PNP. GDP and 'GTP' $KRas^{G12D}$ were rendered SH active by covalent attachment of the SH-active dye, SHG1-SE, to surface-available lysine residues via succinimidyl ester chemistry (14, 15, 17). GDP-bound and 'GTP'-bound $KRas^{G12D}$ conjugates (GDP $KRas^{G12D}$-SHG1 and 'GTP' $KRas^{G12D}$-SHG1) showed degrees of labeling of 1.2 and 0.8 dyes per monomer, respectively, by intact mass spectrometry analysis. The GDP-bound protein yielded a higher degree of labeling compared with the 'GTP' protein, most likely due to the more flexible nature of KRas in its GDP-bound state (23). Mass spectrometry peptide analysis revealed the predominant sites for dye modifications at residues K42, K128, and K147 (Fig. 2*A*), indicative of a heterogeneous conjugated protein population where each molecule carries a single probe distributed among 1 to 2 of these sites. It has been established that labeling at multiple residues allows for sensitive detection of ligand-induced conformational change (16, 18, 20, 21), and we deemed the presence of multiple conjugation sites beneficial for unbiased screening to sample for global and local conformational modulators. To ensure that $KRas^{G12D}$ function was not affected by dye conjugation, Raf-RBD pulldowns were carried out in the presence of unlabeled $KRas^{G12D}$ and $KRas^{G12D}$-SHG1. The Ras effector Raf-RBD specifically recognizes the active GTP-bound nucleotide state. Efficient pulldown of 'GTP'-bound unlabeled $KRas^{G12D}$ and $KRas^{G12D}$-SHG1 using GST-Raf-RBD agarose beads demonstrated that 'GTP' $KRas^{G12D}$-SHG1 protein binds Raf similar to unlabeled protein (Fig. 2*B*).

GDP $KRas^{G12D}$-SHG1 was tethered via its N-terminal His tag to a lipid bilayer-coated surface containing nickel-nitrilotriacetic acid (Ni-NTA) (17, 19), and its baseline SHG signal intensity was recorded. All SHG experiments were carried out by incubating 1 μM $KRas^{G12D}$-SHG1 on the bilayer surface overnight at 4 °C followed by removal of unbound protein. To explore our ability to detect $KRas^{G12D}$ conformational changes in real time using SHG, we monitored the SHG signal intensity of GDP $KRas^{G12D}$-SHG1 on addition of a biological ligand, the nucleotide exchange factor Son of Sevenless (SOS). SOS_{cat} (amino acids 550 to 1,050), the catalytic domain of SOS (24), binds Ras directly with micromolar affinity in solution (25). Increasing concentrations of SOS_{cat} produced a robust concentration-dependent decrease in the SHG signal change, indicative of GDP $KRas^{G12D}$ conformational change on protein–protein binding (25) (Fig. 2*C*).

As an additional positive control for the assay system, we sought to determine whether KRas antibodies caused a change in SHG signal. GDP $KRas^{G12D}$-SHG1 produced a decrease in SHG signal on injection with 3 different commercial anti-Ras antibodies (Fig. 2*D*). Interestingly, the Y13-259 clone, previously characterized to bind Ras residues 70 to 89 (26), produced an SHG signal change almost half the magnitude of the 2 pan-Ras antibodies, MP 05–1072 and MP 05–516, which were each raised against the entire recombinant protein rather than a specific epitope and seem to stabilize the same conformation. No SHG signal change was observed on injection of α-tubulin or

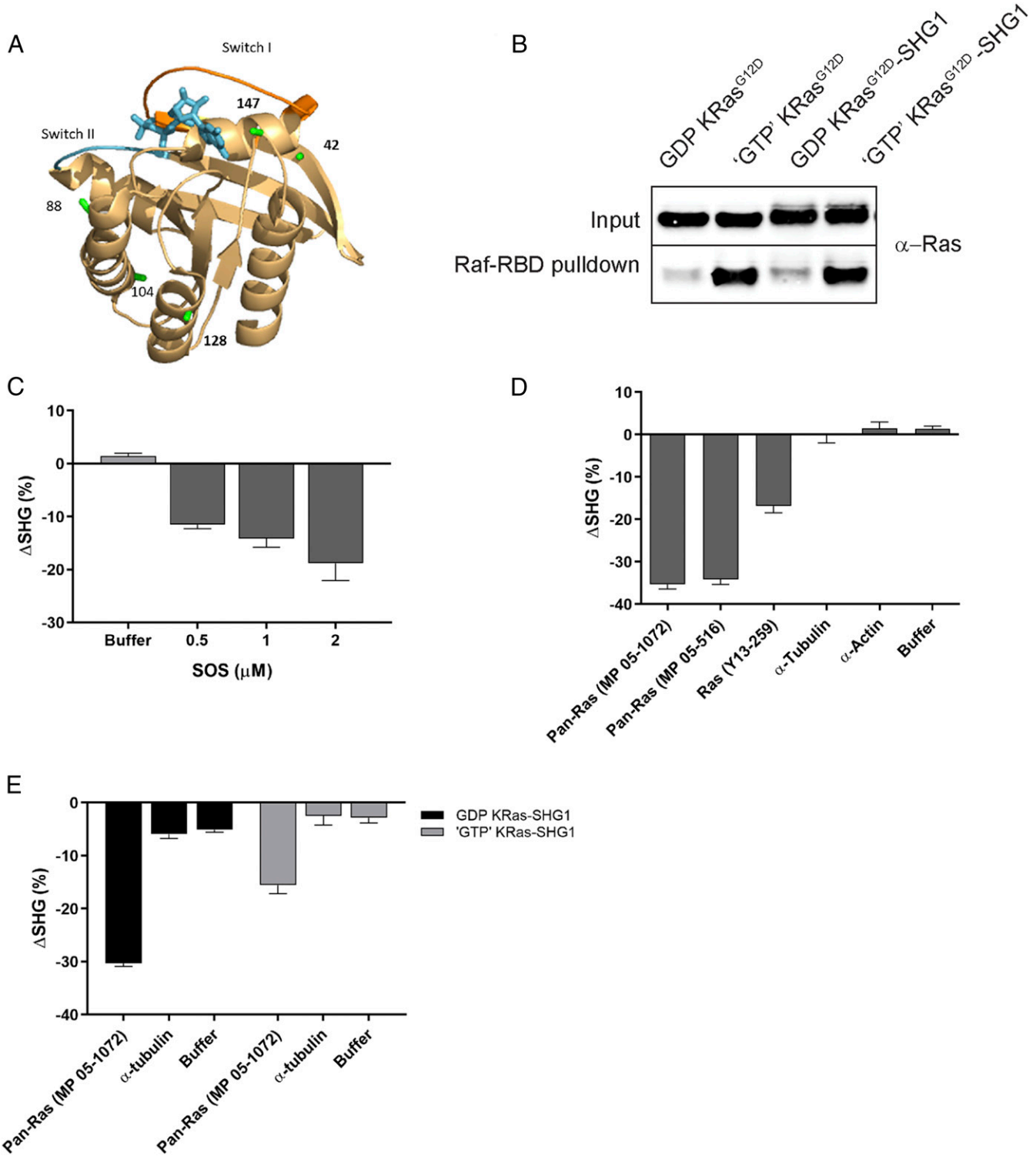

Fig. 2. KRas^{G12D} G-domain SHG assay development. (*A*) KRas^{G12D} structure illustrating the solvent-accessible lysine residues labeled by SHG probe conjugation (green). The dominant labeling sites are indicated in bold. (*B*) GST-Raf-RBD beads were incubated in the presence of unconjugated or SH-active KRas^{G12D} loaded with GDP or 'GTP' as indicated. The reaction input and Ras:Raf-RBD complex was analyzed with anti-Ras antibody. (*C*) His-tagged GDP KRas^{G12D}-SHG1 was tethered to an Ni-NTA bilayer, and the SHG signal intensity was monitored in the presence of increasing SOS_{cat} (micromolar). (*D*) His-tagged GDP KRas^{G12D}-SHG1 was tethered to an Ni-NTA bilayer, and the SHG signal was monitored in the presence of 1 μM buffer-matched monoclonal antibody. (*E*) GDP or 'GTP' KRas^{G12D}-SHG1 was monitored in the presence of 1 μM buffer-matched monoclonal antibody (mean ± SD [error bars]; $n = 3$). All SHG measurements were recorded before and 2 min after ligand addition.

α-actin antibodies (Fig. 2*D*), which do not bind KRas. These results not only demonstrate our ability to detect GDP $KRas^{G12D}$ conformational change on ligand binding, but also highlight how relative differences in the SHG signal changes with the same target reflect distinct ligand-induced conformational changes. The conformational response of 'GTP' $KRas^{G12D}$-SHG1 was also monitored on antibody addition, and robust SHG signal changes were observed in the presence of a pan-Ras antibody, which produced −30.3 ± 0.6% SHG signal change against GDP $KRas^{G12D}$-SHG1 and −15.5 ± 1.6% against 'GTP' $KRas^{G12D}$-SHG1 (Fig. 2*E*). These different SHG responses likely reflect differences in dye conjugation between the GDP- and 'GTP'-bound states.

SHG-Based Screen for Conformational Modulators of Oncogenic $KRas^{G12D}$. Having characterized $KRas^{G12D}$-SHG1 conformational responses in the presence of SOS and antibodies, we sought to identify a small molecule control for 'GTP' $KRas^{G12D}$-SHG1, our primary screen target. In the absence of available high-affinity Ras small molecule binders, we tested a set of promiscuously binding compounds identified from previous unrelated screens. The compound mepazine has been characterized as a mucosa-associated lymphoid tissue lymphoma translocation 1 (MALT1) protease inhibitor (27, 28). For our purposes, 50 μM mepazine produced a −39.3 ± 3.2% signal change compared with −1.3 ± 1.1% upon injection of buffer alone (Fig. 3*A*), and we chose it as a positive control for screening. While not a selective Ras ligand, mepazine produced a consistent and measurable SHG response for monitoring plate-to-plate reproducibility at the time of screening. In a full 384-well plate, 'GTP' $KRas^{G12D}$-SHG1 signal intensity was measured upon injection with buffer or mepazine, and we calculated a Z' factor of 0.6 based on percentage of SHG signal change (ΔSHG [%]). This score reflects a reproducible assay with good separation between positive and negative control responses (29).

We screened a 2,710-fragment collection provided by the University of California San Francisco Small Molecule Discovery Center at 500 and 250 μM ligand concentrations in 2% dimethylsulfoxide (DMSO) against bilayer-tethered 'GTP' $KRas^{G12D}$-SHG1 (Fig. 3*B*). All SHG measurements were acquired before and 2 min after compound injection; 490 compounds produced a saturating or dose-dependent SHG signal change (ΔSHG [%]) >10% or <−10%, our threshold for an initial hit, and these were retested in duplicate at 100 and 20 μM against both the GDP and 'GTP' $KRas^{G12D}$-SHG1 assays. A set of 60 compounds that produced a concentration-dependent SHG response was selected for orthogonal validation by surface plasmon resonance (SPR). SPR analysis was carried out against biotinylated GDP or 'GTP' $KRas^{G12D}$ to assess ligand binding to unconjugated $KRas^{G12D}$. The top 20% of binders (*SI Appendix*, Fig. S1) were selected for additional characterization.

One compound, designated fragment 18 in our study, produced a concentration-dependent positive SHG signal change against both the GDP and 'GTP' $KRas^{G12D}$-SHG1 assays (Fig. 3*C*). Fragment 18, 4-(cyclopent-2-en-1-yl)phenol (Fig. 3*D*), is a para-substituted phenol that is chemically distinct from previously published Ras binders (7, 8, 30). SHG time course measurements revealed that both GDP and 'GTP' $KRas^{G12D}$-SHG1 conjugates produced a maximal signal response 2 min postcompound injection followed by a small decrease that stabilized around 10 min, resulting in signal end point changes relative to baseline of >30% in both nucleotide-bound states (Fig. 3 *C* and *E*). Attempts at determining the binding affinity of fragment 18 to $KRas^{G12D}$ by SPR were carried out, but binding saturation was never reached in the presence of 0 to 500 μM ligand, precluding determination of its binding dissociation constant (K_d). Due to solubility limitations, we were unable to assay >500 μM compound within the DMSO limit of our SPR assay conditions.

NMR Structural Characterization Validates Fragment 18 Binding and Identifies Binding Site. Fragment 18 binding to KRas was characterized by ^{1}H ^{15}N heteronuclear single-quantum coherence (HSQC) spectra analysis of uniformly ^{15}N-labeled GDP $KRas^{G12D}$ in the absence and presence of 0 to 5 mM ligand. GDP $KRas^{G12D}$ $^{1}H/^{15}N$ chemical shifts were monitored in the presence of buffer containing 0, 5, or 10% DMSO, and no significant structural changes were observed due to DMSO (*SI Appendix*, Fig. S2*A*). These conditions allowed us to overcome the solubility limitations encountered in SHG and SPR to monitor chemical shift changes in the presence of millimolar ligand. Fragment 18 produced dose-dependent chemical shift perturbations in residues L56, D57, D69, T74, and G75 as well as smaller perturbations detected at L6, V8, and G10 (Fig. 4*A*). Most of these residues are located within or adjacent to the switch 2 region of $KRas^{G12D}$ (amino acids 60 to 75), where the SOS nucleotide exchange factor binds (31). Quantitative analysis of the dose-dependent chemical shift responses was used to calculate the compound's binding affinity (K_d = 3.3 ± 1.3 mM) (Fig. 4*A* and *SI Appendix*, Fig. S2*B*).

Notably, the $KRas^{G12D}$ chemical shifts observed in the presence of fragment 18 were the same as those described to shift in the presence of 4,6-dichloro-2-methyl-3-aminoethyl-indole (DCAI), a fragment previously reported to bind the KRas SOS binding pocket (8). Since fragment 18 appears to bind the same KRas region, DCAI binding was monitored by SHG and NMR under the same conditions used for fragment 18 analysis. DCAI produced a significant dose-dependent SHG signal change; however, the signal decrease was distinct from the signal increase observed upon fragment 18 binding (Fig. 4*B*), indicating that the 2 compounds induce different conformations of GDP $KRas^{G12D}$-SHG1. The $^{1}H/^{15}N$ KRas spectrum in the presence of 0 to 10 mM DCAI was also different from that observed in the presence of fragment 18. Compound-induced chemical shift perturbations were observed throughout the protein, notably in α-helices 1 and 3 (Fig. 4*A*). These shifts are in addition to those reported for the DCAI binding site on $KRas^{G12D}$ between α-helix 2 and the core β-sheet determined by X-ray crystallography (8), indicating that DCAI binds to multiple sites on KRas in solution.

A predicted binding pose for fragment 18 was generated by the site identification by ligand competitive saturation (SILCS) Monte Carlo (MC) sampling approach (32–34). The crystal structure of $KRas^{G12D}$ (Protein Data Bank [PDB] ID code 4DST) was used to initialize the SILCS simulations to predict protein surface affinity patterns termed FragMaps (35). Analysis of the predicted binding pose of fragment 18 (Fig. 4*C*) shows it to bind in an orientation similar to that of DCAI (8). The cyclopentene and phenyl groups of fragment 18 overlay with apolar FragMaps, while the hydroxyl group overlays with a hydrogen bonding FragMap. The binding of fragment 18 is dominated by hydrophobic contacts between its aromatic and aliphatic rings and hydrophobic KRas residues, including V7, L56, and Y71, with additional hydrogen bonding between its hydroxyl group and the backbone carbonyl oxygen of residue D54. We explored whether fragment 18 affected KRas behavior in biochemical assays but observed no functional effect, likely due to its weak affinity (*SI Appendix*, Fig. S3).

Discussion

We describe the application of a biophysical SHG screening platform to identify conformational modulators of oncogenic $KRas^{G12D}$ from a 2,710-fragment collection. We developed SHG assays for GDP and 'GTP' $KRas^{G12D}$ using SH-active amine-labeled conjugates of this protein. SH-active $KRas^{G12D}$ was monitored for SHG signal detection and response to Ras-specific ligands while ensuring that $KRas^{G12D}$ activity was not impaired by incorporation of the SHG probe. We report the identification of a Ras binder from our primary SHG screen and describe how

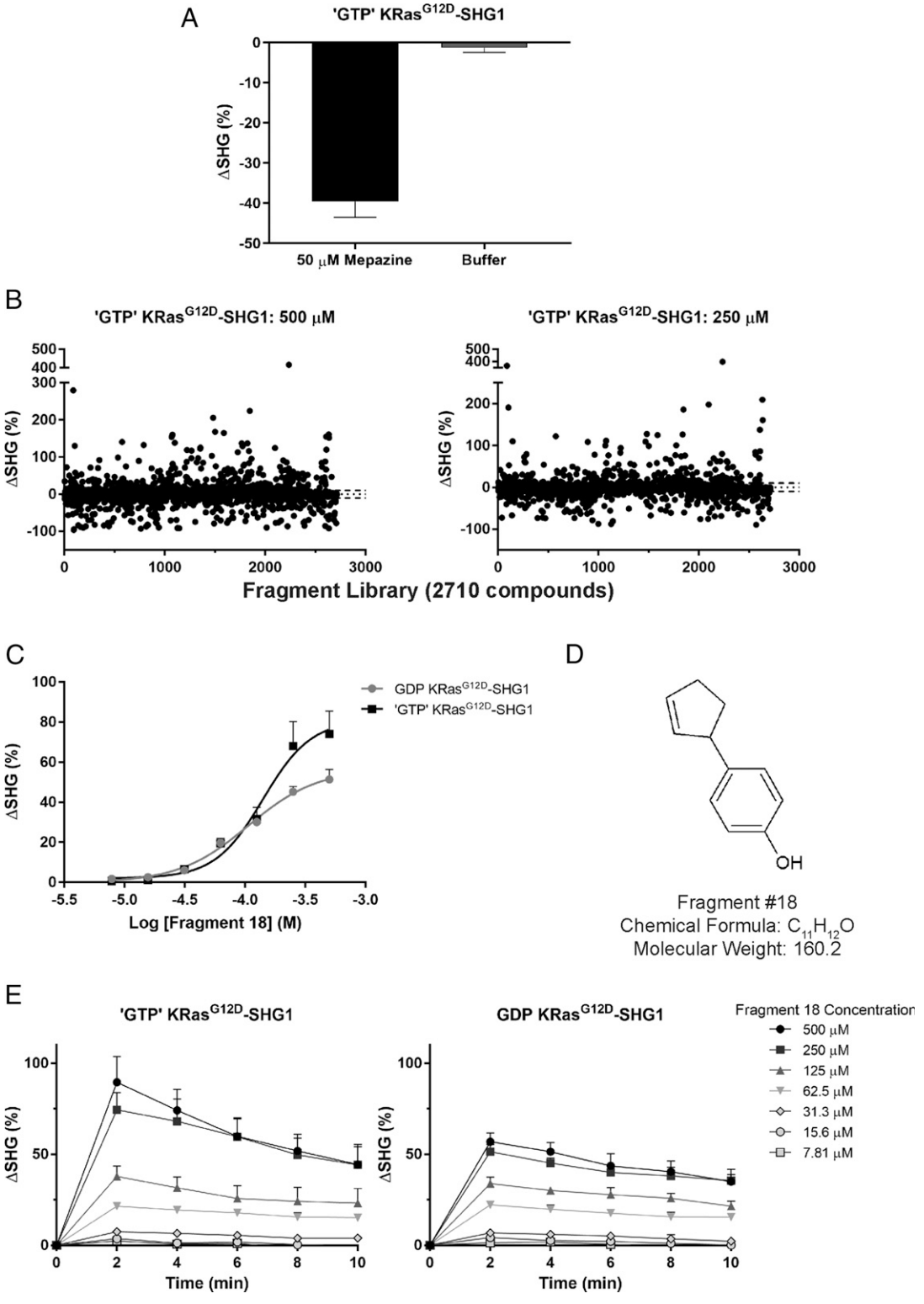

Fig. 3. Primary SHG-based screen reveals the KRas^{G12D} fragment ligand. (*A*) The percentage SHG signal change (ΔSHG [%]) was monitored in the presence or absence of 50 μM mepazine in a 384-well Biodesy Delta plate 2 min postinjection. (*B*) 'GTP' KRas^{G12D}-SHG1 SHG signal change in the presence of (*Left*) 500 or (*Right*) 250 μM fragment concentration across the library. The dotted lines indicate ±10% threshold. (*C*) Fragment 18 concentration response curve at T = 4 min postinjection (mean ± SD [error bars]; $n = 3$). (*D*) The chemical structure of fragment 18, 4-(cyclopent-2-en-1-yl)phenol. (*E*) The SHG signals of (*Left*) 'GTP' KRas^{G12D}-SHG1 and (*Right*) GDP KRas^{G12D}-SHG1 were monitored in the presence of 0 to 500 μM fragment 18 for 10 min, with measurements taken at 2-min intervals postinjection.

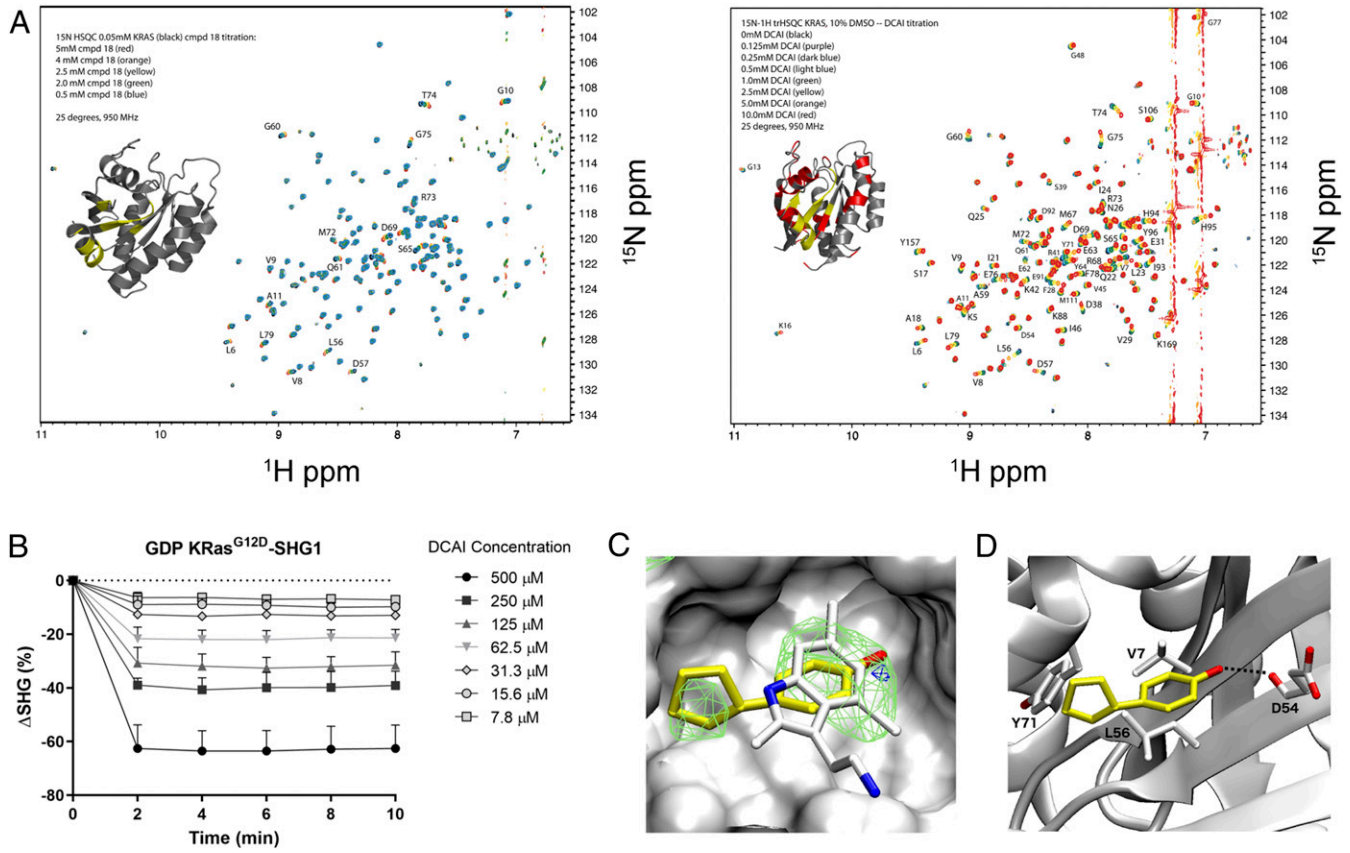

Fig. 4. The 2D ^{1}H ^{15}N TROSY HSQC NMR validates fragment (cmpd) 18 binding to KRas^{G12D}. (*A*) The ^{1}H ^{15}N TROSY HSQC NMR spectra of 50 μM GDP KRas^{G12D} in the presence of increasing ligand concentration. The KRas^{G12D} ribbon model shows the predicted binding interface in yellow. (*Left*) TROSY HSQC GDP KRas^{G12D} spectra in the presence of 0 to 5 mM fragment 18. (*Right*) TROSY HSQC GDP KRas^{G12D} spectra in the presence of 0 to 10 mM DCAI. KRas^{G12D} ribbon model shows the predicted DCAI binding interface in yellow and red. (*B*) GDP KRas^{G12D}-SHG1 10-min SHG time course in the presence of 0 to 500 μM DCAI. (*C*) Fragment 18 docking to KRas^{G12D} in DCAI pocket. The docking pose of fragment 18 (yellow carbon atoms) was predicted with SILCS FragMaps and overlaid on the crystal binding mode of DCAI (white carbon atoms; PDB ID code 4DST). The apolar (green) and hydrogen bonding donor (blue) FragMaps are shown in the KRas^{G12D} small molecule binding pocket (surface in white) overlapping corresponding functional groups from both compounds. (*D*) Predicted binding pose of fragment 18 and its interactions with surrounding KRas residues.

SHG characterization provides additional insights into conformational dynamics that otherwise require resource-intensive techniques less amenable to primary screening.

SHG measures relative conformational movement, and different ligands can produce different signals at the same occupancy. We loosened traditional screening constraints to select 18% of our fragment library for secondary SHG screening at lower concentrations. Hits were funneled through additional iterations of single-concentration SHG KRas assays at 100 and 20 μM ligand. The top 60 candidate ligands were assayed by SPR to reveal <10 fragments for structural characterization by NMR (*SI Appendix*). We encountered technical challenges to validate ligand binding to KRas^{G12D} by SPR due to the combination of weak ligand affinity and solubility thresholds that precluded our ability to reach binding saturation. To overcome these limitations, we applied 2-dimensional (2D) HSQC NMR on uniformly labeled ^{15}N GDP KRas^{G12D} with conditions that allowed for significantly higher ligand concentrations. NMR analysis in the presence of fragment 18 confirmed ligand binding to a distinct region of KRas^{G12D} with an observed K_d around 3 mM (Fig. 4). Identifying a 3 mM KRas^{G12D} binder from a primary screen at 500 μM (~10% occupancy) highlights the sensitivity of SHG.

Fragment 18, 4-(cyclopent-2-en-1-yl)phenol, produced dose-dependent chemical shifts in KRas^{G12D} residues L56, D57, D69, T74, and G75. The reported chemical shifts were the same as those described upon the characterization of DCAI as a fragment binder to a hydrophobic pocket between KRas^{G12D} α-helix 2 and its core β-sheet with 1 mM affinity (8). SILCS-MC docking simulations predict that fragment 18 binds the KRas^{G12D} SOS binding pocket in a similar orientation to DCAI. Despite the fact that fragment 18 and DCAI bind the same pocket, they produced distinct KRas^{G12D} conformational changes by SHG (Figs. 3 and 4). Using HSQC NMR to explore specific KRas^{G12D} structural changes in the presence of DCAI, we observed evidence of previously unreported chemical shifts in KRas^{G12D} α-helices 1 and 3 (Fig. 4*A*). The HSQC spectra in the presence of fragment 18 clearly localized to a single distinct region in the SOS binding pocket (Fig. 4*A*). Although DCAI was discovered by NMR fragment screening, Maurer et al. (8) used X-ray crystallography to characterize its binding site. We suspect that crystals were unable to form when bound by multiple DCAI molecules. The HSQC NMR structural results illustrate how, unlike SPR or saturation transfer difference-nuclear magnetic resonance (STD-NMR), SHG provides both binding information and conformational data in a solution-based dynamic system. We attempted to cocrystallize GDP KRas^{G12D} with fragment 18, but no ligand-bound crystals formed, presumably due to its weak binding affinity.

In biochemical assays, fragment 18 did not impact KRas^{G12D} effector binding or KRas^{G12D} SOS-mediated nucleotide exchange (*SI Appendix*, Fig. S3). These observations are consistent with a previous study where indole fragments bound to the SOS binding pocket only inhibited SOS-mediated nucleotide exchange with affinities <500 μM (7, 9). In contrast, DCAI was reported to inhibit SOS-mediated nucleotide exchange despite

exceeding this 500 μM affinity threshold (8). Our NMR-based structural data illustrate that DCAI binds additional sites outside the SOS binding pocket, and we suspect that these additional interactions inhibit KRas function by another mechanism.

The discovery of chemical matter that binds KRas in a single and well-defined pocket is quite valuable as we explore approaches to identify ligands and study the range of Ras conformational changes (22, 36). Fragment 18 induced a distinct positive SHG signal change against $KRas^{G12D}$ with a maximal conformational response at 2 min. Previous crystallographic data of unbound and indole-bound KRas suggest that this hydrophobic pocket only opens in the presence of ligand (7), consistent with our SHG conformational data showing an immediate conformational change on fragment 18 binding followed by a second conformational rearrangement.

SHG has emerged as a biophysical technique for detecting conformational change in biological targets, including those characterized as undruggable due to disordered structural elements or to a lack of obvious binding pockets (18, 20). SHG intensity is highly dependent on the angular orientation of the probe relative to the surface plane, thus measuring both local and global conformational changes (17, 21). In this study, we labeled surface-exposed lysine residues to monitor ligand-induced conformational change and successfully identified a ligand to a site with no immediately adjacent SH-active dye conjugated site, reflecting the tightly coordinated structural dynamics of Ras proteins (36, 37). $KRas^{G12D}$ ligand binding characterized by SHG revealed distinct conformational changes induced by fragment 18 or DCAI that would not have been immediately apparent using other biophysical methods. We illustrate how SHG can be used both as a primary screening platform and to provide conformational insight that complements traditional structural techniques. Furthermore, there are intensive efforts to build selective ligands from low-affinity fragment binders to shallow or inducible pockets, and we have demonstrated that SHG is a powerful platform for this type of application.

Materials and Methods

Protein Labeling with SH-Active Dye. GDP- or 'GTP'-bound His-tagged $KRas^{G12D}$ (1-166; $KRas^{G12D}$) was lysine labeled with SH-active dye (SHG1-SE; Biodesy, Inc.) via succinimidyl ester chemistry. $KRas^{G12D}$ was buffer exchanged into 100 mM $NaHCO_3$, pH 8.3, 150 mM NaCl, 1 mM $MgCl_2$, and 0.5 mM tris (2-carboxyethyl)phosphine (TCEP). KRas was labeled at 50 μM with an 8:1 dye to protein molar ratio. The reaction was terminated by buffer exchange with ZebaSpin Desalting Columns, 7 K molecular weight cutoff (MWCO), 0.5 mL (Thermo Scientific) into 40 mM 4-(2-hydroxyethyl)-1-piperazineethanesulfonic acid (Hepes), pH 8.0, 150 mM NaCl, 1 mM $MgCl_2$, and 1 mM TCEP.

SHG Assay Preparation and Measurements. Supported lipid bilayers containing Ni-NTA were prepared according to the manufacturer's instructions (Biodesy, Inc.) and were formed by fusion to the well surface of 384-well Biodesy plates (17). GDP- or 'GTP'-bound $KRas^{G12D}$-SHG1 was tethered to the lipid bilayer membrane at a concentration of 1 μM in KRas assay buffer (40 mM Hepes, pH 8.0, 150 mM NaCl, 1 mM $MgCl_2$) and incubated overnight at 4 °C. After it was tethered, wells were washed with assay buffer to remove unbound protein (17, 20, 21).

Ligand injections and SHG detection were carried out on the Biodesy Delta as follows: after reading the baseline SHG signal, 20 μL of ligand at 2 times the desired concentration was injected onto 20 μL of solution volume. The SHG signal change was defined as the percentage change in SHG intensity, ΔSHG (%), and calculated as $((I_t - I_{t0})/I_{t0}) \times 100$, where I_t is the SHG intensity at time t and I_{t0} is the SHG baseline intensity before injection (17, 18, 20). *SI Appendix, SI Materials and Methods* has details on instrumentation.

NMR Sample Preparation. NMR samples contained 50 μM uniformly ^{15}N-labeled KRas in 50 mM Hepes, pH 7.4, 150 mM NaCl, 2 mM $MgCl_2$, 1 mM TCEP, 10% D_2O, and 5 to 10% D6-DMSO with and without varying concentrations of putative small molecule inhibitors.

HSQC NMR. All NMR experiments were acquired at 298 K on a Bruker Avance III 950-MHz spectrometer equipped with a *z*-gradient cryogenic probe. A series of 2D [^1H ^{15}N] transverse relaxation optimized spectroscopy (TROSY) HSQCs was collected at increasing compound concentrations. NMR data were processed with NMRPipe. All proton chemical shifts were referenced to external trimethylsilyl propanoic acid at 25 °C (0.00 ppm) with respect to residual H_2O (4.698 ppm). ^1H to ^{15}N chemical shifts were indirectly referenced using a 0-point frequency ratio of 0.101329118.

Docking Study. The SILCS approach was performed using the Grand Canonical MC/molecular dynamics protocol (32–35). The crystal structure of the KRas G12D mutant (PDB ID code 4DST) was solvated in a water box containing 8 representative solutes at 0.25 M concentration with different chemical functionalities (benzene, propane, acetaldehyde, methanol, formamide, imidazole, acetate, and methylammonium) to probe the functional group requirements of the protein. From the SILCS simulations, 3-dimensional fragment probability distributions (FragMaps) were generated, normalized, and converted to grid free energy FragMaps as previously described (32–35). *SI Appendix, SI Materials and Methods* has details.

Protein Expression and Purification, Nucleotide Loading, and Biochemical Assays. *SI Appendix, SI Materials and Methods* has details.

ACKNOWLEDGMENTS. Research reported in this publication was supported by the Office of The Director, NIH Award S10OD023482, NIH/National Cancer Institute T32 Training Program Grant T32 CA108462 (to E.D.), and a Daiichi Sankyo grant (to F.M.). This project has been funded in whole or in part by federal funds from National Cancer Institute, NIH Contract HHSN261200800001E. We thank University of California, San Francisco Small Molecule Discovery Center for providing the fragment library and compound management support, specifically Michelle Arkin and Kenny Ang. Adam Renslo provided tool compounds. Matt Duncton provided medicinal chemistry analysis. We also thank John Kuriyan and Yasushi Kondo (University of California, Berkeley) for providing SOS_{cat}. We thank members of the Protein Expression Laboratory (Frederick National Laboratory for Cancer Research) for their help in cloning, protein expression, and purification, specifically John-Paul Denson, Dominic Esposito, Peter Frank, Bill Gillette, Gulcin Gultin, Jennifer Mehalko, Simon Messing, Nitya Ramakrishnan, Troy Taylor, and Vanessa Wall. The content of this publication does not necessarily reflect the views or policies of the Department of Health and Human Services nor does mention of trade names, commercial products, or organizations imply endorsement by the US Government.

1. J. M. Ostrem, K. M. Shokat, Direct small-molecule inhibitors of KRAS: From structural insights to mechanism-based design. *Nat. Rev. Drug Discov.* **15**, 771–785 (2016).
2. S. Gysin, M. Salt, A. Young, F. McCormick, Therapeutic strategies for targeting ras proteins. *Genes Cancer* **2**, 359–372 (2011).
3. F. McCormick *et al.*, Interaction of ras p21 proteins with GTPase activating protein. *Cold Spring Harb. Symp. Quant. Biol.* **53**, 849–854 (1988).
4. A. G. Stephen, D. Esposito, R. K. Bagni, F. McCormick, Dragging ras back in the ring. *Cancer Cell* **25**, 272–281 (2014).
5. A. D. Cox, S. W. Fesik, A. C. Kimmelman, J. Luo, C. J. Der, Drugging the undruggable RAS: Mission possible? *Nat. Rev. Drug Discov.* **13**, 828–851 (2014).
6. F. McCormick, Progress in targeting RAS with small molecule drugs. *Biochem. J.* **476**, 365–374 (2019).
7. Q. Sun *et al.*, Discovery of small molecules that bind to K-Ras and inhibit Sos-mediated activation. *Angew. Chem. Int. Ed. Engl.* **51**, 6140–6143 (2012).
8. T. Maurer *et al.*, Small-molecule ligands bind to a distinct pocket in Ras and inhibit SOS-mediated nucleotide exchange activity. *Proc. Natl. Acad. Sci. U.S.A.* **109**, 5299–5304 (2012).
9. M. C. Burns *et al.*, Approach for targeting Ras with small molecules that activate SOS-mediated nucleotide exchange. *Proc. Natl. Acad. Sci. U.S.A.* **111**, 3401–3406 (2014).
10. M. R. Janes *et al.*, Targeting KRAS mutant cancers with a covalent G12C-specific inhibitor. *Cell* **172**, 578–589.e17 (2018).
11. M. P. Patricelli *et al.*, Selective inhibition of oncogenic KRAS output with small molecules targeting the inactive state. *Cancer Discov.* **6**, 316–329 (2016).
12. J. M. Ostrem, U. Peters, M. L. Sos, J. A. Wells, K. M. Shokat, K-Ras(G12C) inhibitors allosterically control GTP affinity and effector interactions. *Nature* **503**, 548–551 (2013).
13. R. J. Tran, K. L. Sly, J. C. Conboy, Applications of surface second harmonic generation in biological sensing. *Annu. Rev. Anal. Chem. (Palo Alto, Calif.)* **10**, 387–414 (2017).
14. J. S. Salafsky, Detection of protein conformational change by optical second-harmonic generation. *J. Chem. Phys.* **125**, 074701 (2006).
15. J. S. Salafsky, 'SHG-labels' for detection of molecules by second harmonic generation. *Chem. Phys. Lett.* **342**, 485–491 (2001).
16. J. S. Salafsky, Second-harmonic generation for studying structural motion of biological molecules in real time and space. *Phys. Chem. Chem. Phys.* **9**, 5704–5711 (2007). Erratum in: *Phys. Chem. Chem. Phys.* **9**, 6047 (2007).
17. B. Moree *et al.*, Protein conformational changes are detected and resolved site specifically by second-harmonic generation. *Biophys. J.* **109**, 806–815 (2015).

18. B. Moree *et al*., Small molecules detected by second-harmonic generation modulate the conformation of monomeric α-synuclein and reduce its aggregation in cells. *J. Biol. Chem.* **290**, 27582–27593 (2015).
19. T. A. Young *et al*., Second-harmonic generation (SHG) for conformational measurements: Assay development, optimization, and screening. *Methods Enzymol.* **610**, 167–190 (2018).
20. M. T. Butko, B. Moree, R. B. Mortensen, J. Salafsky, Detection of ligand-induced conformational changes in oligonucleotides by second-harmonic generation at a supported lipid bilayer interface. *Anal. Chem.* **88**, 10482–10489 (2016).
21. J. J. W. Wong *et al*., Monomeric ephrinB2 binding induces allosteric changes in Nipah virus G that precede its full activation. *Nat. Commun.* **8**, 781 (2017).
22. N. Bery *et al*., Correction: BRET-based RAS biosensors that show a novel small molecule is an inhibitor of RAS-effector protein-protein interactions. *eLife* **7**, e40515 (2018). Erratum in: *eLife* **7**, e37122 (2018).
23. J. Ma, M. Karplus, Ligand-induced conformational changes in ras p21: A normal mode and energy minimization analysis. *J. Mol. Biol.* **274**, 114–131 (1997).
24. S. M. Margarit *et al*., Structural evidence for feedback activation by Ras.GTP of the Ras-specific nucleotide exchange factor SOS. *Cell* **112**, 685–695 (2003).
25. U. Vo *et al*., Monitoring Ras interactions with the nucleotide exchange factor Son of sevenless (Sos) using site-specific NMR reporter signals and intrinsic fluorescence. *J. Biol. Chem.* **291**, 1703–1718 (2016).
26. J. C. Lacal, S. A. Aaronson, Activation of ras p21 transforming properties associated with an increase in the release rate of bound guanine nucleotide. *Mol. Cell. Biol.* **6**, 4214–4220 (1986).
27. D. Nagel *et al*., Pharmacologic inhibition of MALT1 protease by phenothiazines as a therapeutic approach for the treatment of aggressive ABC-DLBCL. *Cancer Cell* **22**, 825–837 (2012).
28. C. Mc Guire *et al*., Pharmacological inhibition of MALT1 protease activity protects mice in a mouse model of multiple sclerosis. *J. Neuroinflammation* **11**, 124 (2014).
29. J. H. Zhang, T. D. Chung, K. R. Oldenburg, A simple statistical parameter for use in evaluation and validation of high throughput screening assays. *J. Biomol. Screen.* **4**, 67–73 (1999).
30. M. C. Burns *et al*., High-throughput screening identifies small molecules that bind to the RAS:SOS:RAS complex and perturb RAS signaling. *Anal. Biochem.* **548**, 44–52 (2018).
31. P. A. Boriack-Sjodin, S. M. Margarit, D. Bar-Sagi, J. Kuriyan, The structural basis of the activation of Ras by Sos. *Nature* **394**, 337–343 (1998).
32. E. P. Raman, W. Yu, S. K. Lakkaraju, A. D. MacKerell, Jr, Inclusion of multiple fragment types in the site identification by ligand competitive saturation (SILCS) approach. *J. Chem. Inf. Model.* **53**, 3384–3398 (2013).
33. W. Yu, S. K. Lakkaraju, E. P. Raman, L. Fang, A. D. MacKerell, Jr, Pharmacophore modeling using site-identification by ligand competitive saturation (SILCS) with multiple probe molecules. *J. Chem. Inf. Model.* **55**, 407–420 (2015).
34. W. Yu, S. K. Lakkaraju, E. P. Raman, A. D. MacKerell, Jr, Site-identification by ligand competitive saturation (SILCS) assisted pharmacophore modeling. *J. Comput. Aided Mol. Des.* **28**, 491–507 (2014).
35. O. Guvench, A. D. MacKerell Jr, Computational evaluation of protein-small molecule binding. *Curr. Opin. Struct. Biol.* **19**, 56–61 (2009).
36. C. I. Nnadi *et al*., Novel K-Ras G12C switch-II covalent binders destabilize Ras and accelerate nucleotide exchange. *J. Chem. Inf. Model.* **58**, 464–471 (2018).
37. C. W. Johnson *et al*., The small GTPases K-Ras, N-Ras, and H-Ras have distinct biochemical properties determined by allosteric effects. *J. Biol. Chem.* **292**, 12981–12993 (2017).